CIRFA
CENTRE FOR
INTEGRATED REMOTE SENSING
AND FORECASTING FOR ARCTIC OPERATIONS

Keynote:

Applications of full-polarimetric SAR to monitoring newly formed sea ice, leads, and oil spills

Professor Camilla Brekke

ESA Cryosphere Remote Sensing Training Course 2018
Longyearbyen, Svalbard, 12 June

cirfa.uit.no

Topic 1: Sea ice observations – From a HP SAR perspective

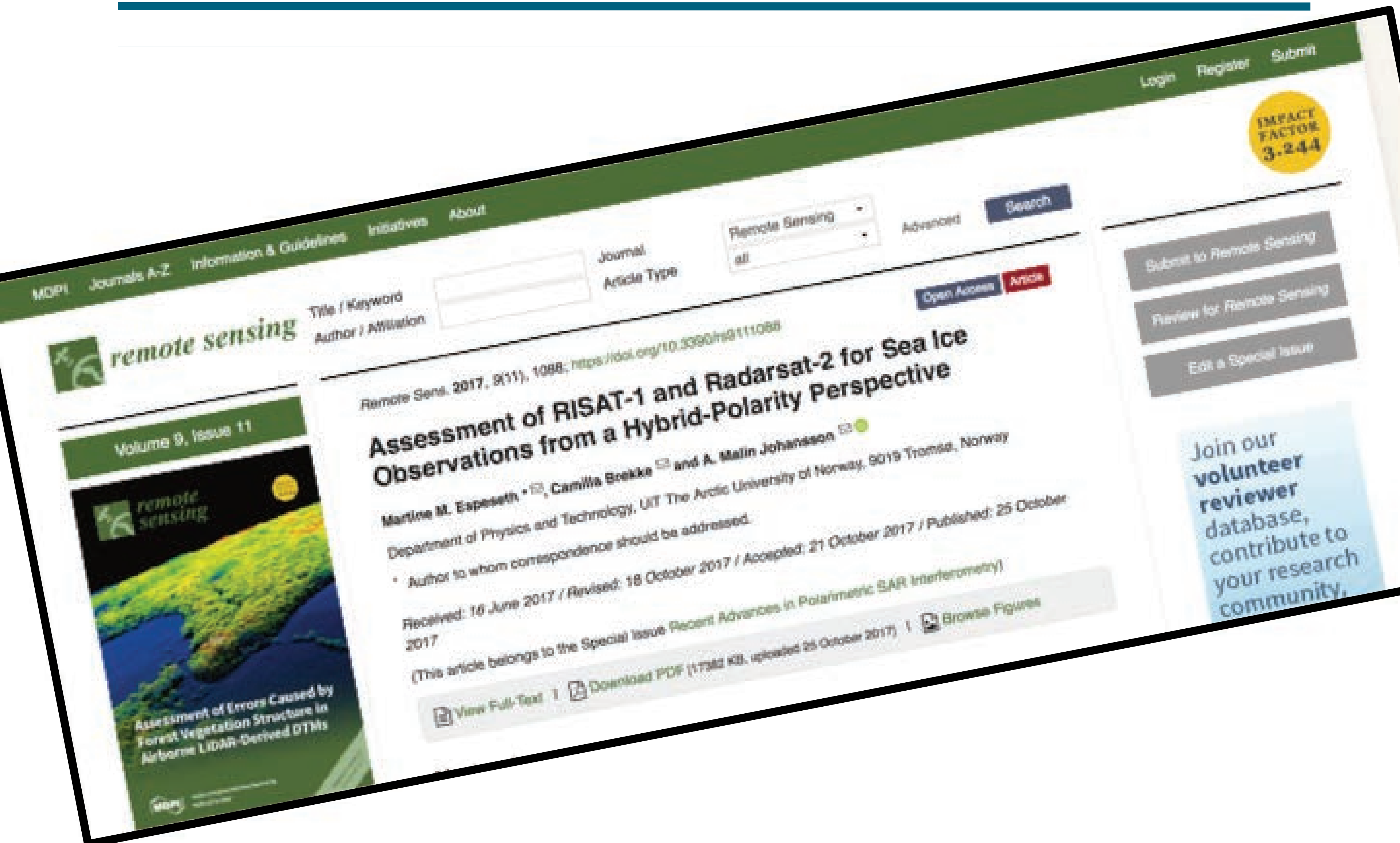

Utilizing several SAR missions provides higher temporal resolution for sea ice studies

Objective of study:

- Establish knowledge about the differences between various available SAR sensors and polarization modes.
- Homogenize the data sets for a uniform and consistent analysis across sensors.

Missions considered:

Radar Imaging Satellite-1 (RI-1), **HP SAR**, Indian (2012-2017)

Radarsat-2 (RS-2), **QP SAR**, Canadian (2007-)

➢ Simulated vs. real HP SAR data for sea ice type separation.

Overlapping simulated (RS-2) and real HP (RI-1) data – Negligable change in conditions within a pair

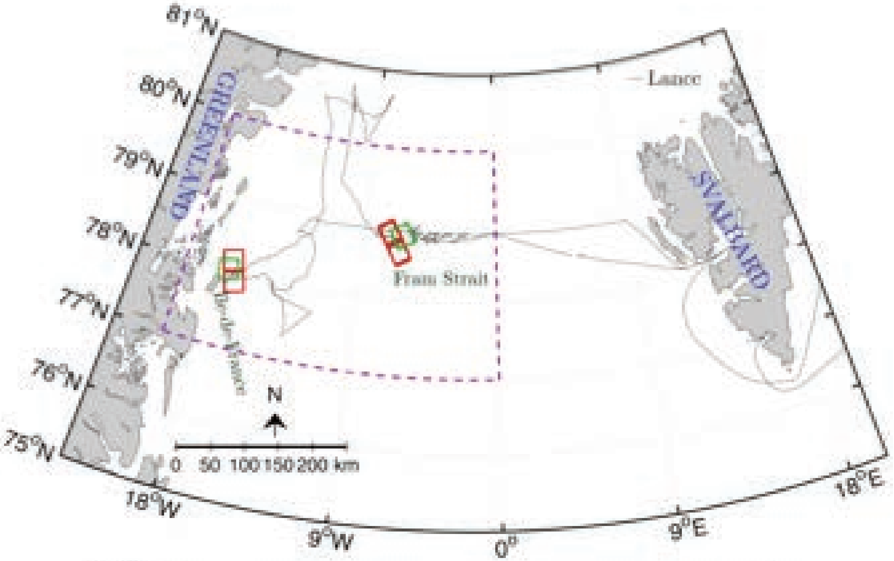

Pair	Satellite	Date	Time (UTC)	Polarization Mode (Beam)
P_1	RI-1 RS-2	6 Sept. 6 Sept.	16:38 16:55	HP (FRS-1) FP (FQ-13)
P_2	RI-1 RS-2	6 Sept. 6 Sept.	18:13 18:35	HP (FRS-1) FP (FQ-29)
P_3	RI-1 RS-2	7 Sept. 7 Sept.	16:30 16:26	HP (FRS-1) FP (FQ-5)

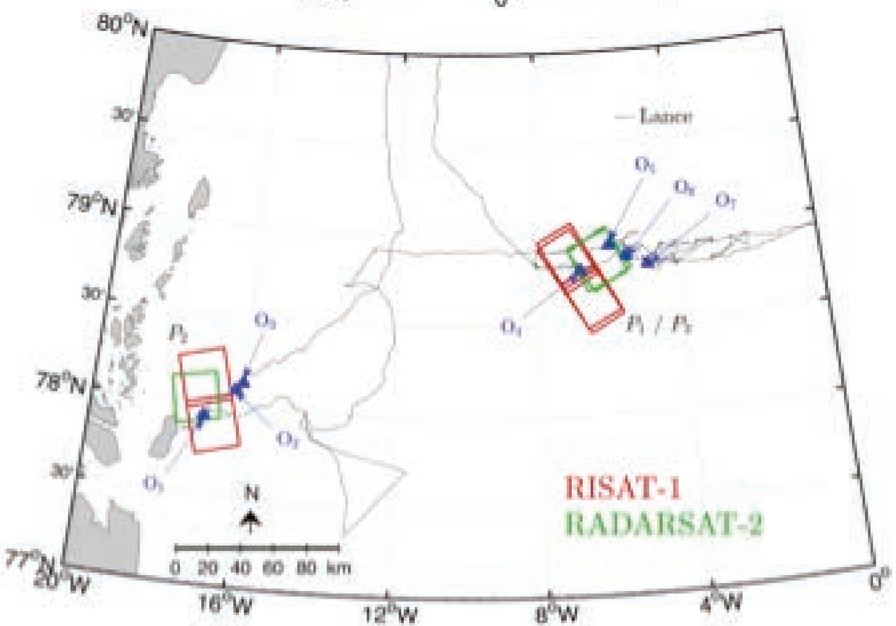

Area	ID	Date (Time) (UTC)	Observations
Ile-de-France (P_2)	O_1	30.08 (22:19)	Newly formed ice and nilas (0.5–5 cm) with snow cover
	O_2	31.08 (11:48)	Newly formed ice and nilas (0.5–4 cm) with snow cover
	O_3	31.08 (12:42)	Leads (2–3 cm), 110–235 cm thick ice and 5–8 cm snow cover
Fram Strait (P_1 and P_3)	O_4	05.09 (11:20)	Scattered floes with 1–2 cm snow cover, melt ponds, and 137–210 cm thick ice
	O_5	06.09 (07:25)	Newly formed frazil/ grease ice (3–4 cm)
	O_6	06.09 (12:56)	High melt pond coverage, 2 cm snow, and 104–187 cm thick ice
	O_7	07.09 (07:42)	Snowfall, 3–4 cm fresh snow layer, and 116–130 cm thick ice

Observations 5 days prior to RI-1/RS-2 acquisitions – Sentinel-1 scenes confirm stable conditions

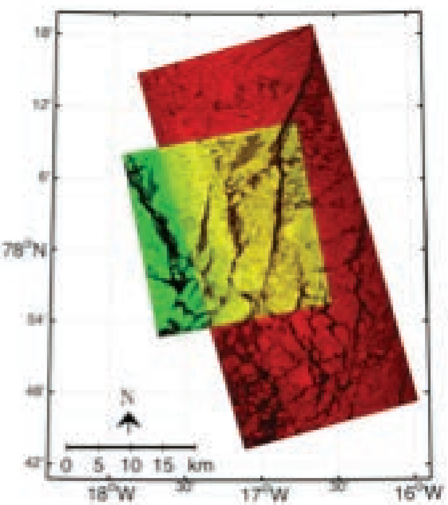

RI-1 RV

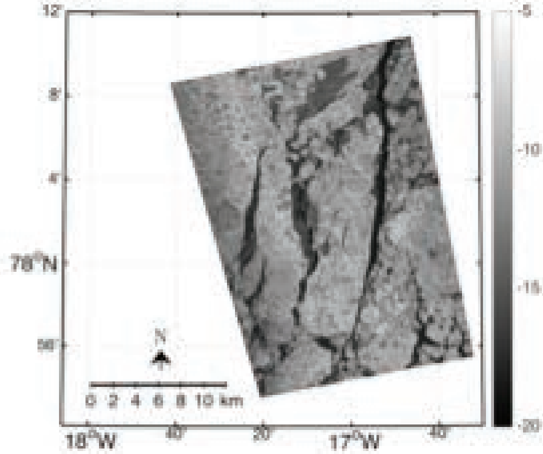

RS-2 VV

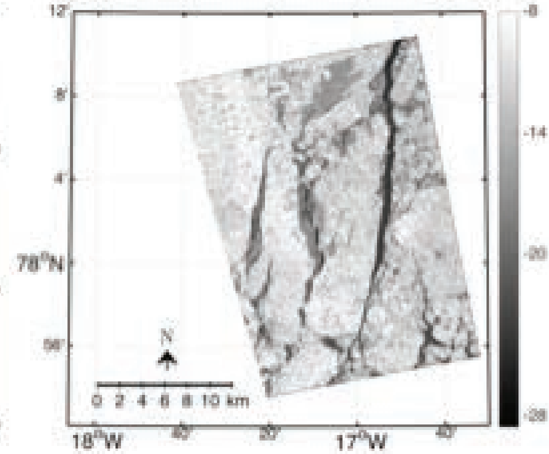

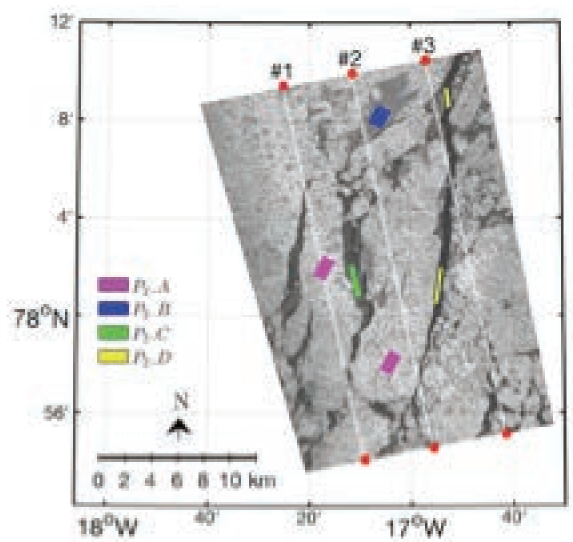

ROIs (Sea Ice Types)
P_2_A (FYI)
P_2_B (Flooded FYI)
P_2_C (Nilas/newly formed ice with snow cover)
P_2_D (Leads)

Non-circularity of the transmitted wave – Effect investigated in relation to sea ice type separability

HP scattering vector:

$$\bar{k}_{(RH,RV)} = [S_{RH}, S_{RV}]^T$$

Simulated HP (RS-2) compared to real HP (RI-1)

$$\bar{k}_{(RH,RV)} = \frac{1}{\sqrt{2}}[S_{HH} - iS_{HV}, -iS_{VV} + S_{HV}]^T.$$

Non-circularity property (RI-1): Not possible to generate perfect circular polarization on transmit using current technology.

RI-1 configuration:

$$\chi = -38^\circ$$
$$\psi = 0^\circ$$

Perfect circular configuration:

$$\chi = -45^\circ$$
$$\psi = 0^\circ$$

$$\bar{k}_{(RH,RV)} = [\cos(\chi)S_{HH} + i\sin(\chi)S_{HV}, i\sin(\chi)S_{VV} + \cos(\chi)S_{HV}]^T$$

HP features within a group predominately sensitive to common scattering types

Group Number	HP Features	Dominant Scattering Type
Group 1	σ_{RH} σ_{RV} σ_{RL} q_0 q_3	Surface scattering
Group 2	σ_{RR}	Depolarzation due to volume scattering
Group 3	$1-m$ $\gamma_{(RR,RL)}$ $\rho_{(RH,RV)}$	Depolarization due to multiscattering from rough surfaces
Group 4	$\gamma_{(RH,RV)}$	Polarization differences in resonant Bragg scattering and also in the Fresnel coefficients.
Independent group	q_1 q_2 α_s	Might be complementary to other parameters

Kolmogorov-Smirnov (KS) test applied to each feature to evaluate the separability between the sea ice types.

RI-1 and RS-2 HP $\chi = -45^{\circ}$ – All sea ice types separable

$KS \in [0,1]. KS = 0 \; --> \textit{the two cumulative distributions are equal.}$

FYI flooded and nilas with snow

	Group name	HP features	P_2_A vs. P_2_B		P_2_A vs. P_2_C		P_2_A vs. P_2_D		P_2_B vs. P_2_C		P_2_B vs. P_2_D		P_2_C vs. P_2_D	
			RI-1	RS-2	RI-1	RS-2	RI-1	RS-2	RI-1	RS-2	RI-1	RS-2	RI-1	RS-2
	Group 1	σ_{RH}(dB)	0.98	0.99	1.00	1.00	1.00	1.00	0.93	0.85	1.00	1.00	1.00	1.00
Surface scattering		σ_{RV}(dB)	0.98	0.99	1.00	1.00	1.00	1.00	0.61	0.29	1.00	1.00	1.00	1.00
		σ_{RL}(dB)	0.98	0.99	1.00	1.00	1.00	1.00	0.98	0.89	1.00	1.00	1.00	1.00
		q_0(dB)	0.98	0.99	1.00	1.00	1.00	1.00	0.91	0.69	1.00	1.00	1.00	1.00
		q_3(dB)	0.95	0.94	1.00	1.00	1.00	1.00	0.99	0.97	1.00	1.00	0.87	0.94
Depolarization due to volume scattering	Group 2	σ_{RR}(dB)	0.97	0.99	0.99	0.99	1.00	1.00	0.23	0.64	1.00	1.00	0.99	0.99
	Group 3	$1-m$	0.44	0.81	0.83	0.10	0.97	0.56	0.97	0.88	1.00	0.97	0.74	0.55
		$\gamma_{(RR,RL)}$	0.30	0.80	0.89	0.38	0.97	0.67	0.97	0.97	1.00	0.97	0.59	0.49
		$\rho_{(RH,RV)}$	0.46	0.81	0.81	0.16	0.97	0.67	0.97	0.90	1.00	0.97	0.76	0.65
	Group 4	$\gamma_{(RH,RV)}$	0.03	0.12	0.59	0.56	0.68	0.66	0.62	0.67	0.71	0.75	0.11	0.13
	Independent group	q_1(dB)	0.63	0.64	0.80	0.59	0.91	0.86	0.47	0.14	0.75	0.50	0.36	0.60
		q_2(dB)	0.39	0.60	0.58	0.49	0.87	0.91	0.52	0.37	0.97	0.75	0.86	0.93
		a_s(dB)	0.37	0.27	0.70	0.67	0.61	0.63	0.63	0.87	0.57	0.82	0.15	0.13

Group 1 & 2 holds the most powerful features.

Separability between sea ice types similar for both RS-2 HP $\chi = -45^{\circ}$ and $\chi = -38^{\circ}$ (green and blue)

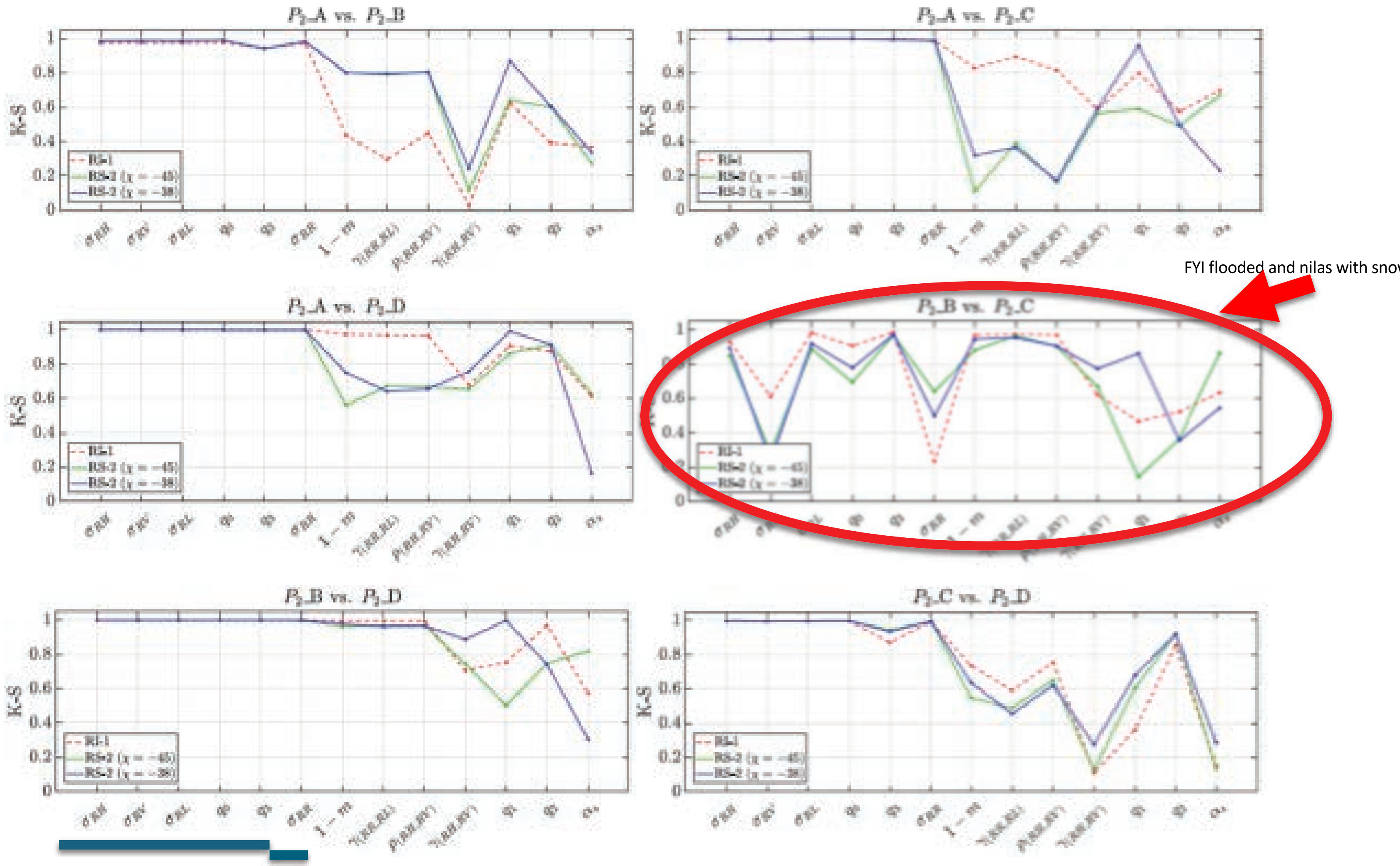

Group 1

Group 2

Why are some features affected by the non-circularity property?

Summary – Sea ice type discrimination in HP SAR

- Real HP vs. simulated HP; comparable performance.
- A more elliptical wave on transmit will not affect the separability of the investigated sea ice types given that the correct features are selected.
- HP features sensitive to *surface scattering* and *depolarization due to volume scattering* have great potential for discrimination.
- These feature groups also contain features with highest discrimination power and invariance to the non-circularity property on transmit.

Topic 2: Sea ice observations – From a multifrequency SAR perspective

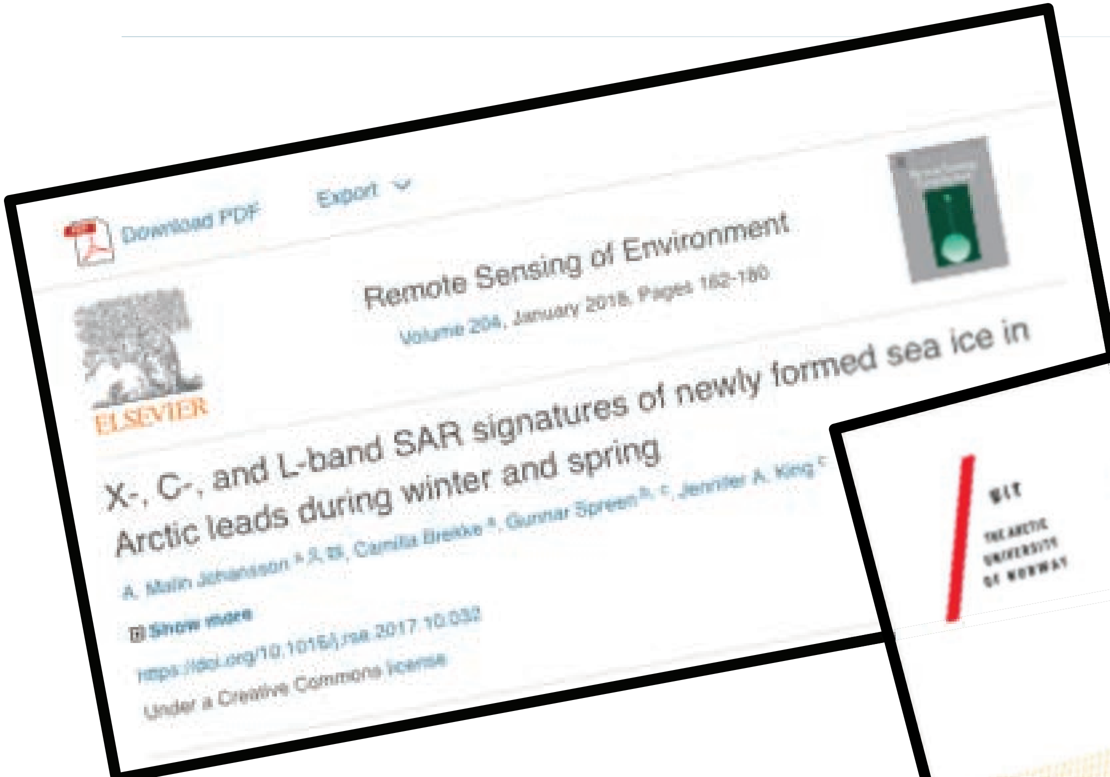

Norwegian young sea ICE 2015 (N-ICE2015) expedition with R/V Lance January – June 2015.

- Satellite data
  - ALOS-2 (L-band)
  - Radarsat-2 (C-band)
  - TerraSAR-X (X-band)
- In-situ data from airborne platforms
  - Electromagnetic soundings
  - Photographs
  - Lidar surface measurements
- Meteorological observations
  - On board the vessel
  - On the sea ice

Photo: Michal Krzysztofowics


Photo: S. Gerland

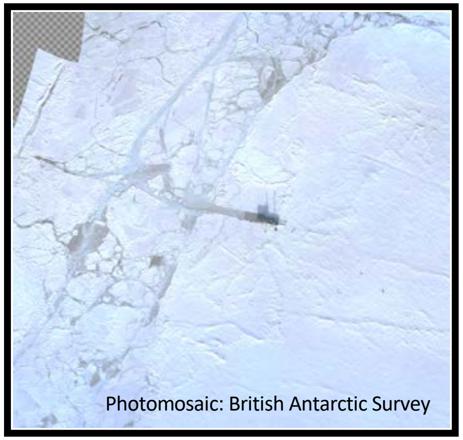
Photomosaic: British Antarctic Survey


Photo: Camilla Brekke

Several near coincident QP SAR acquisitions (pairs or triplets) collected during N-ICE2015.

9 TerraSAR-X

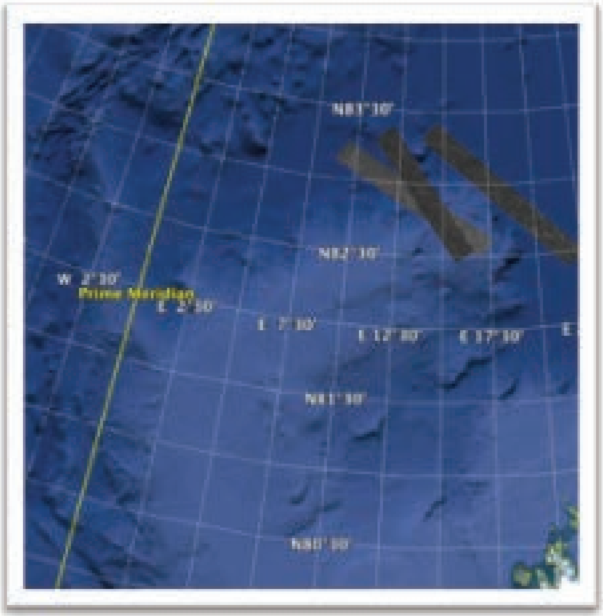

32 Radarsat-2

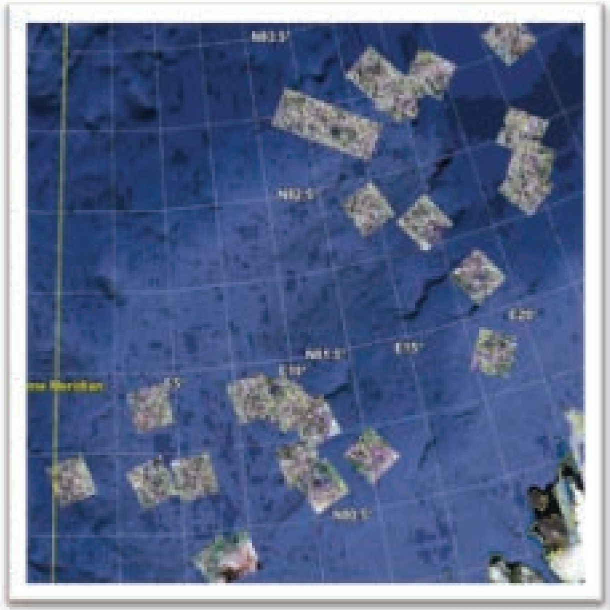

45 ALOS-2

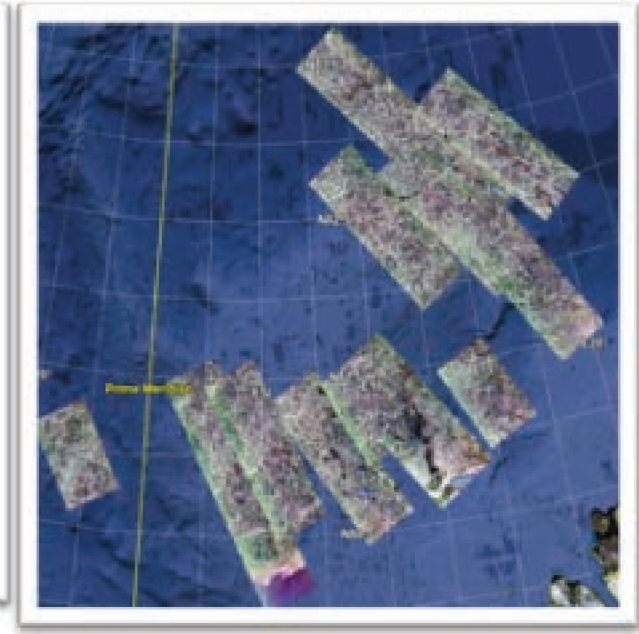

Mission	Band	Incidence angle	Resolution (rg x az)	Width	Length
TerraSAR-X	9.65 GHz/3.1 cm (X-band)	18°-46°	1.2 m x 6 m	18.5 km	55 km
Radarsat-2	5.41 GHz/5.6 cm (C-band)	18°-50°	5.2 m x 7.6 m	25 km	25 km
ALOS-2	1.20 GHz/22.9 cm (L-band)	29°-41°	5.1 m x 4.3 m	40 km – 50 km	70 km

Frost flower covered lead in ALOS-2 vs Radarsat-2 scenes. Entropy higher in Part I (Part II) for C-band (L-band).

C-band 14:42 UTC ---> zoom-in

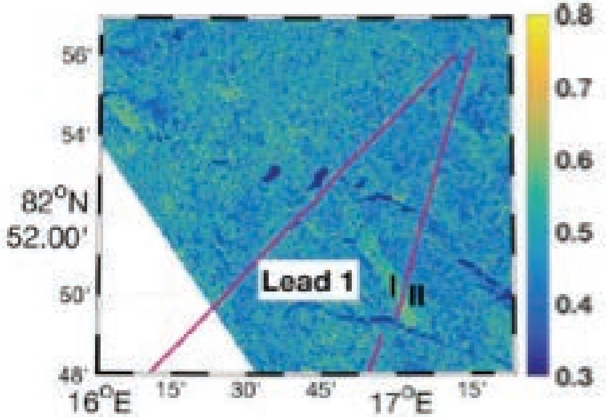

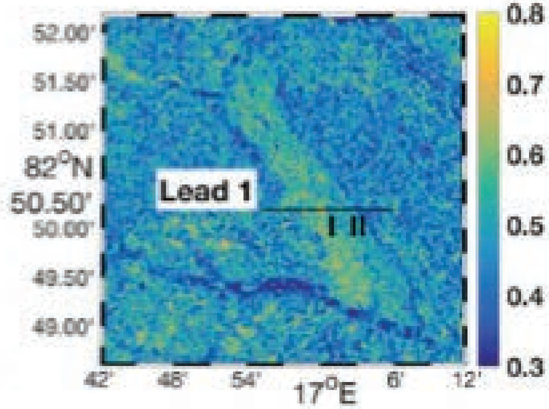

I: Newly formed, small scale surface structures.
Mean snow/ice thickness: 0.3 m.

40 m

40 m

L-band 20:18 UTC ---> zoom-in

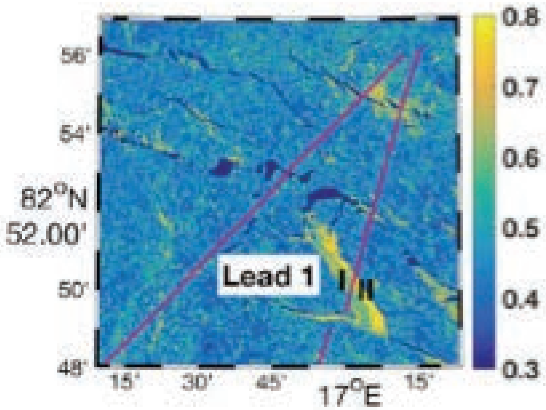

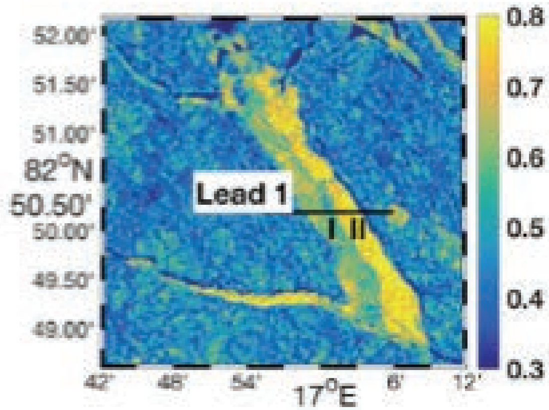

II: Newly formed, smooth.
Mean snow/ice thickness: 0.23 m.

A. M. Johansson, C. Brekke, G. Spreen, and J. A. King, “X-, C-, and L-band SAR signatures of newly formed sea ice in Arctic leads during winter and spring”, *Remote Sensing of Environment*, 2018.

Combinations of SAR frequency bands may give additional information about sea ice medium.

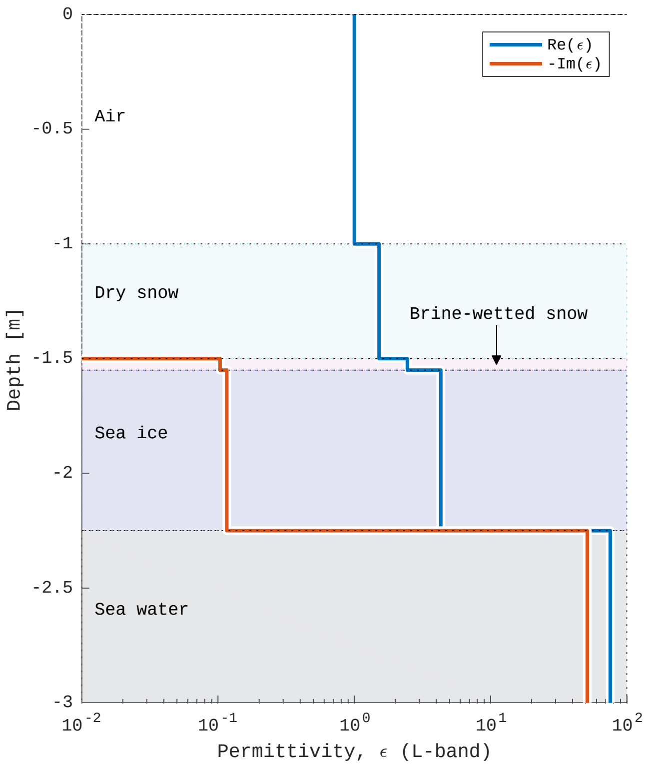

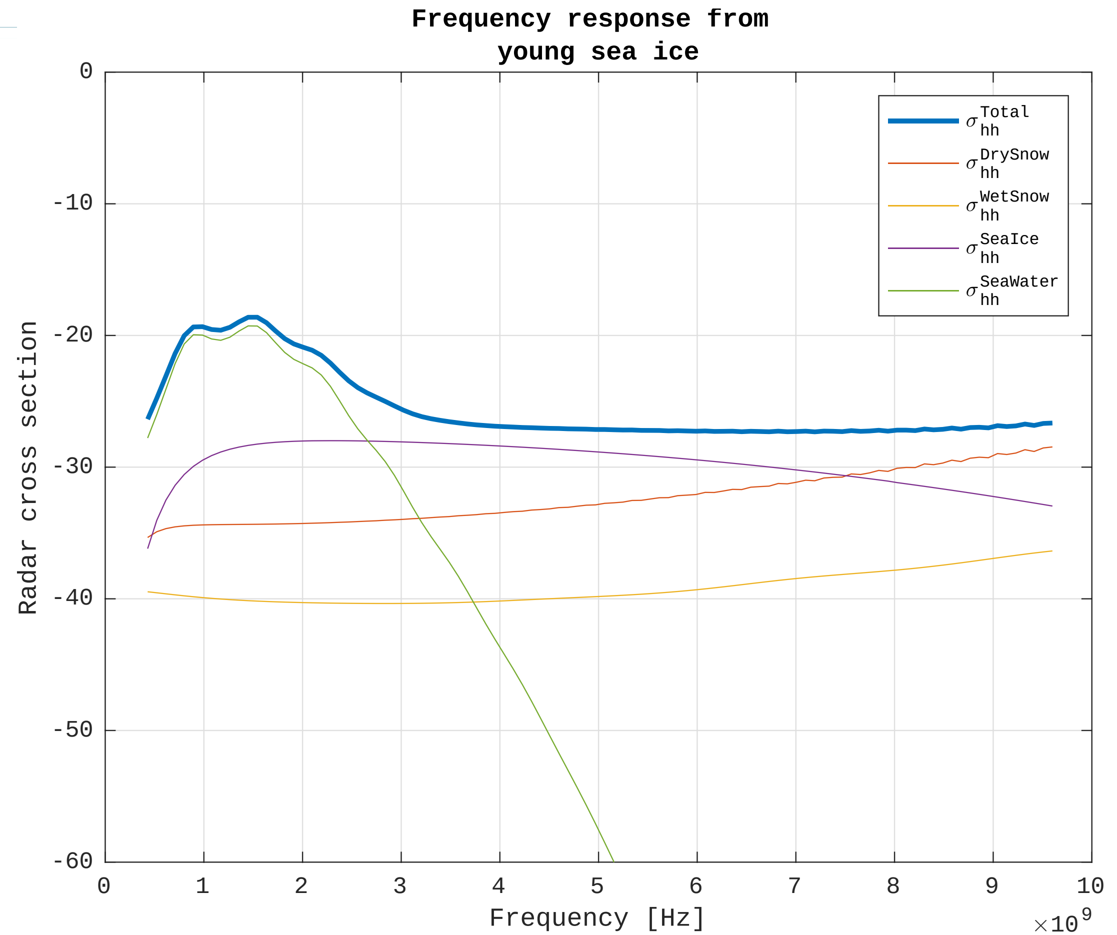

POLARIMETRIC REMOTE SENSING OF GEOPHYSICAL MEDIA WITH LAYER RANDOM MEDIUM MODEL

S. V. Nghiem, M. Borgeaud, J. A. Kong, and R. T. Shin

Dominant:

L-band — Ice-water interface

C-band — Snow-ice interface

X-band — Dry-Snow

Jakob Grahn, "Sea ice remote sensing with multi-frequency radar", PhD thesis, 2018.

Can models aid interpretation of sea ice in ALOS-2 L-band SAR imagery?

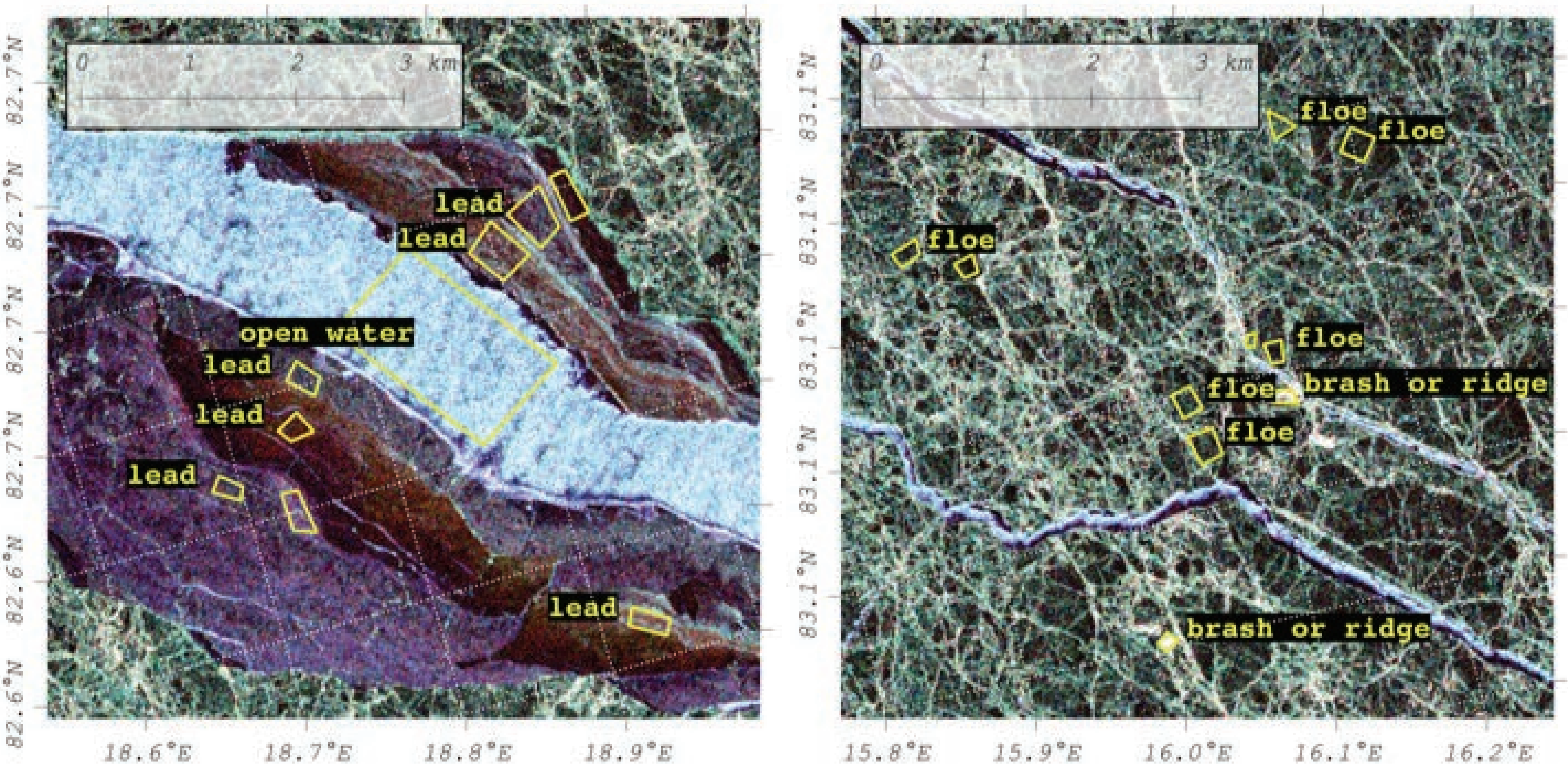

HV

HH

VV

Jakob Grahn, "Sea ice remote sensing with multi-frequency radar", PhD thesis, 2018.

L-band: "Lead ice" data points compared to model. Model overlap – ambiguous interpretation.

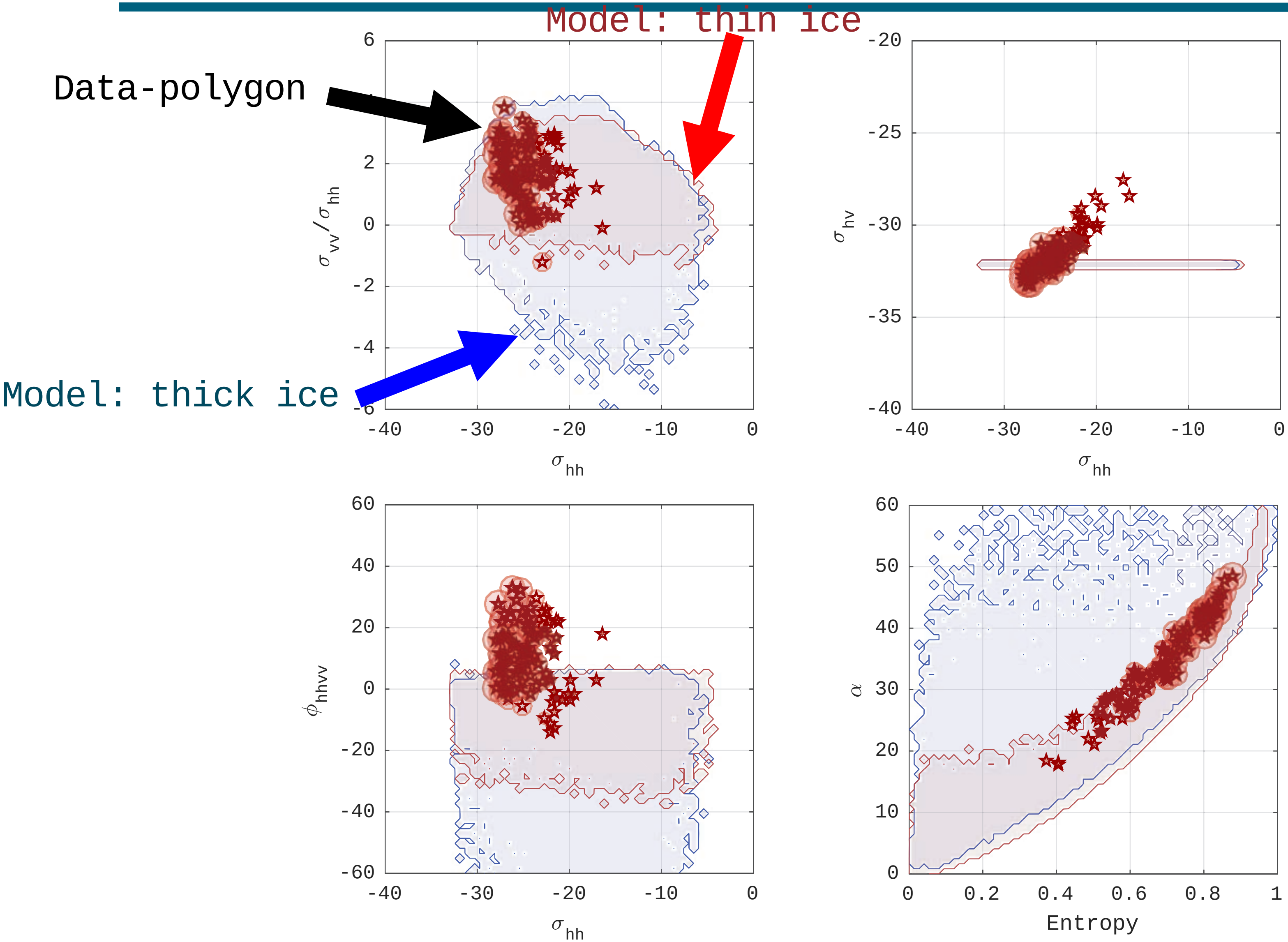

Jakob Grahn, "Sea ice remote sensing with multi-frequency radar", PhD thesis, 2018.

L-band: "Ice floe" data points compared to model. Classification of thin vs thick level ice may be challenging.

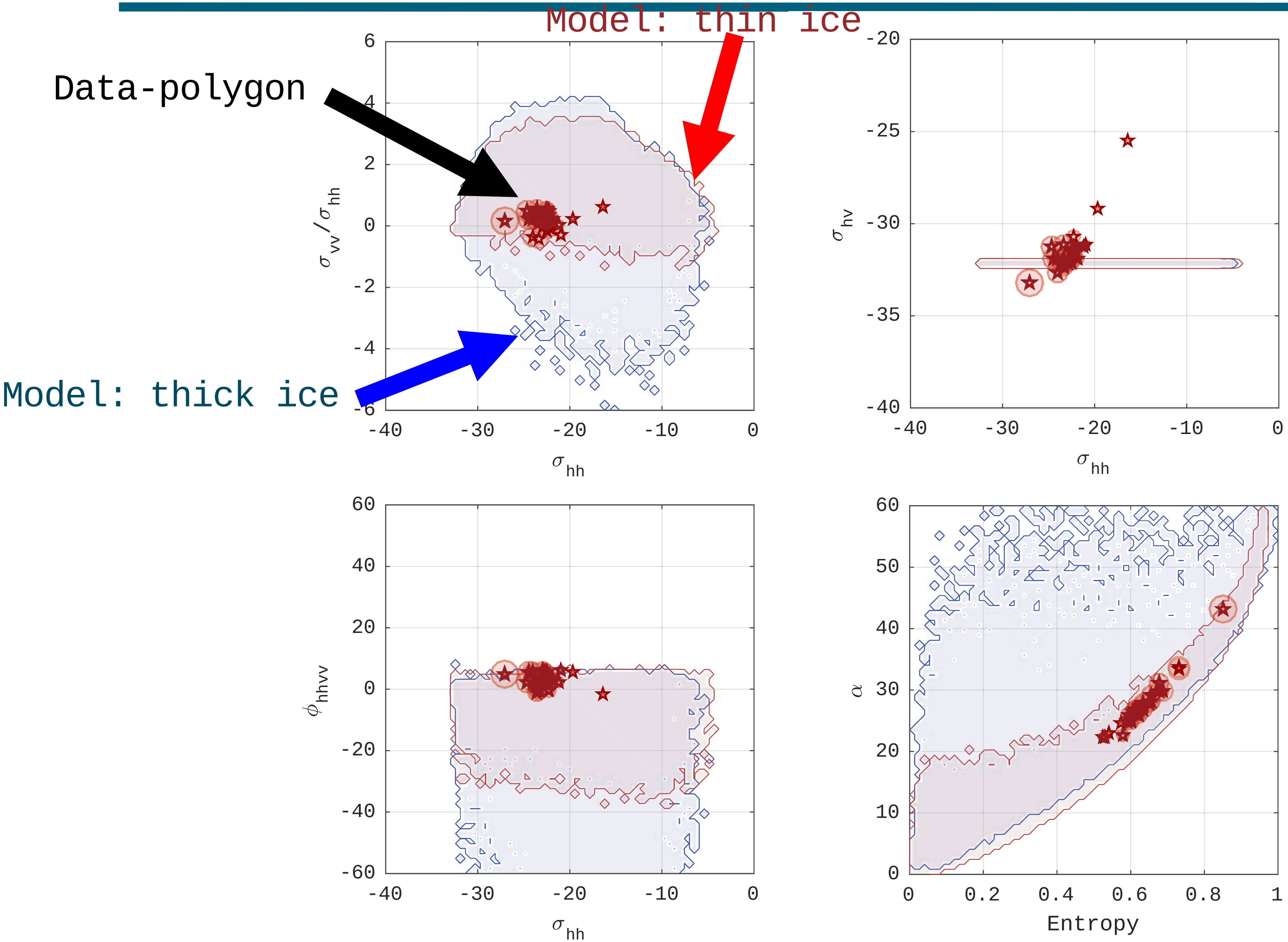

Jakob Grahn, "Sea ice remote sensing with multi-frequency radar", PhD thesis, 2018.

“Open water” observations reveal much lower response in C-band as compared to L-band.

ALOS-2 L-band

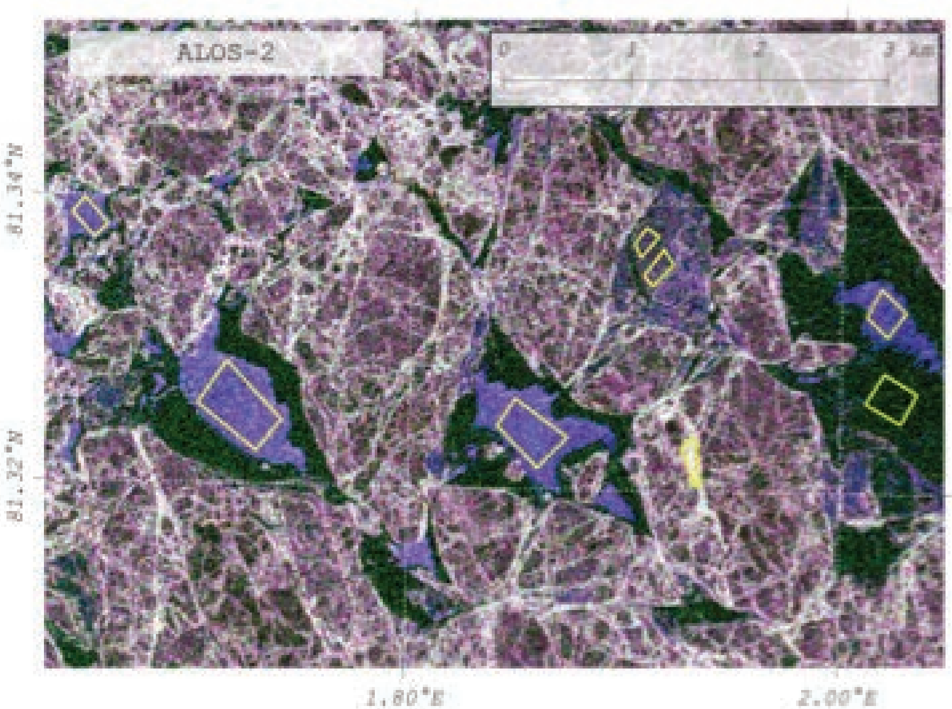

RADARSAT-2 C-band

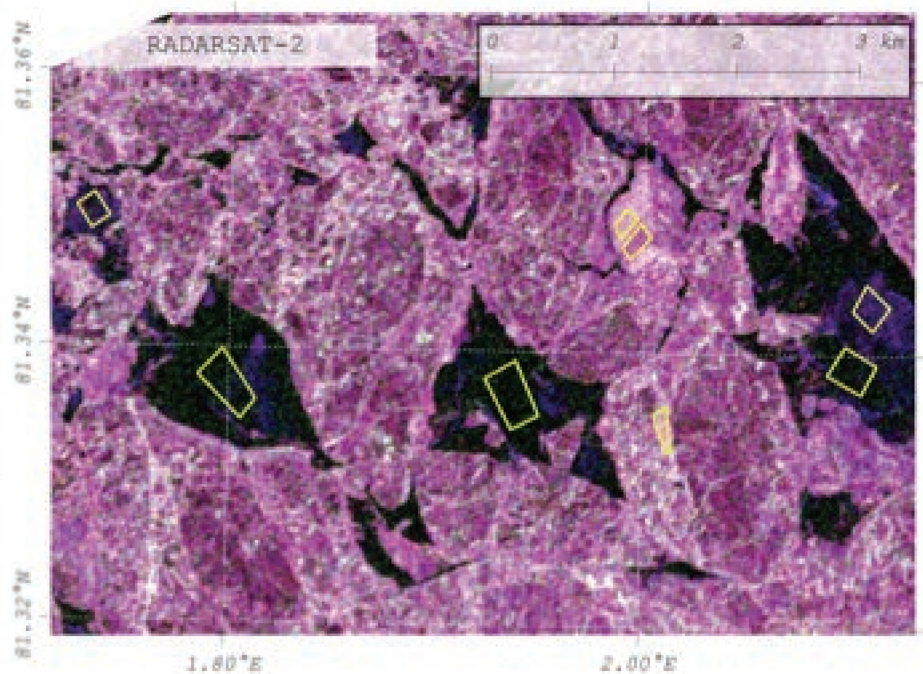

HV

HH

VV

Jakob Grahn, "Sea ice remote sensing with multi-frequency radar”, PhD thesis, 2018.

Is this due to frazil/grease ice slicks?

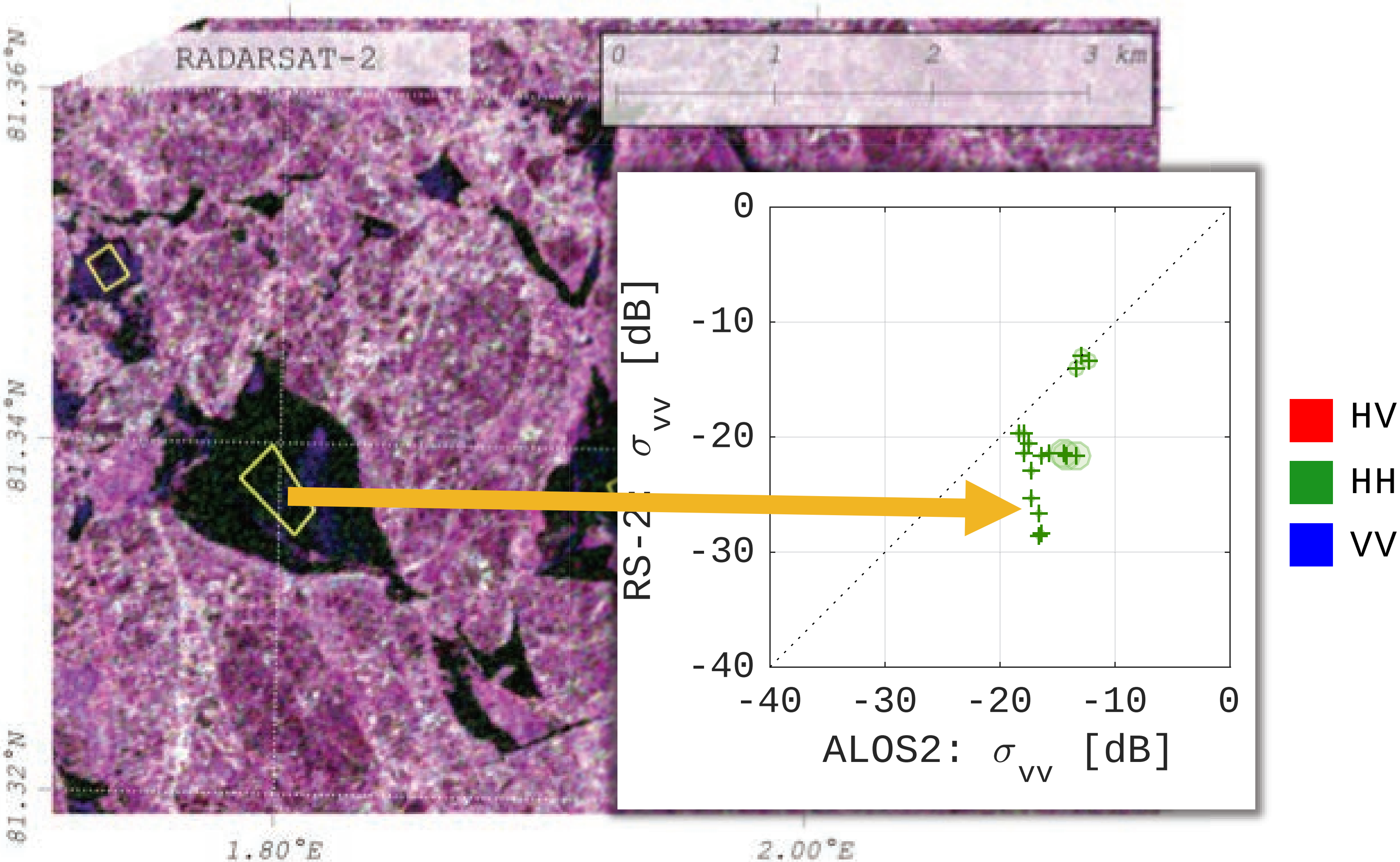

Jakob Grahn, "Sea ice remote sensing with multi-frequency radar", PhD thesis, 2018.

For low viscous slicks, damping at C-band Bragg waves up to two orders of magnitude stronger than at L-band.

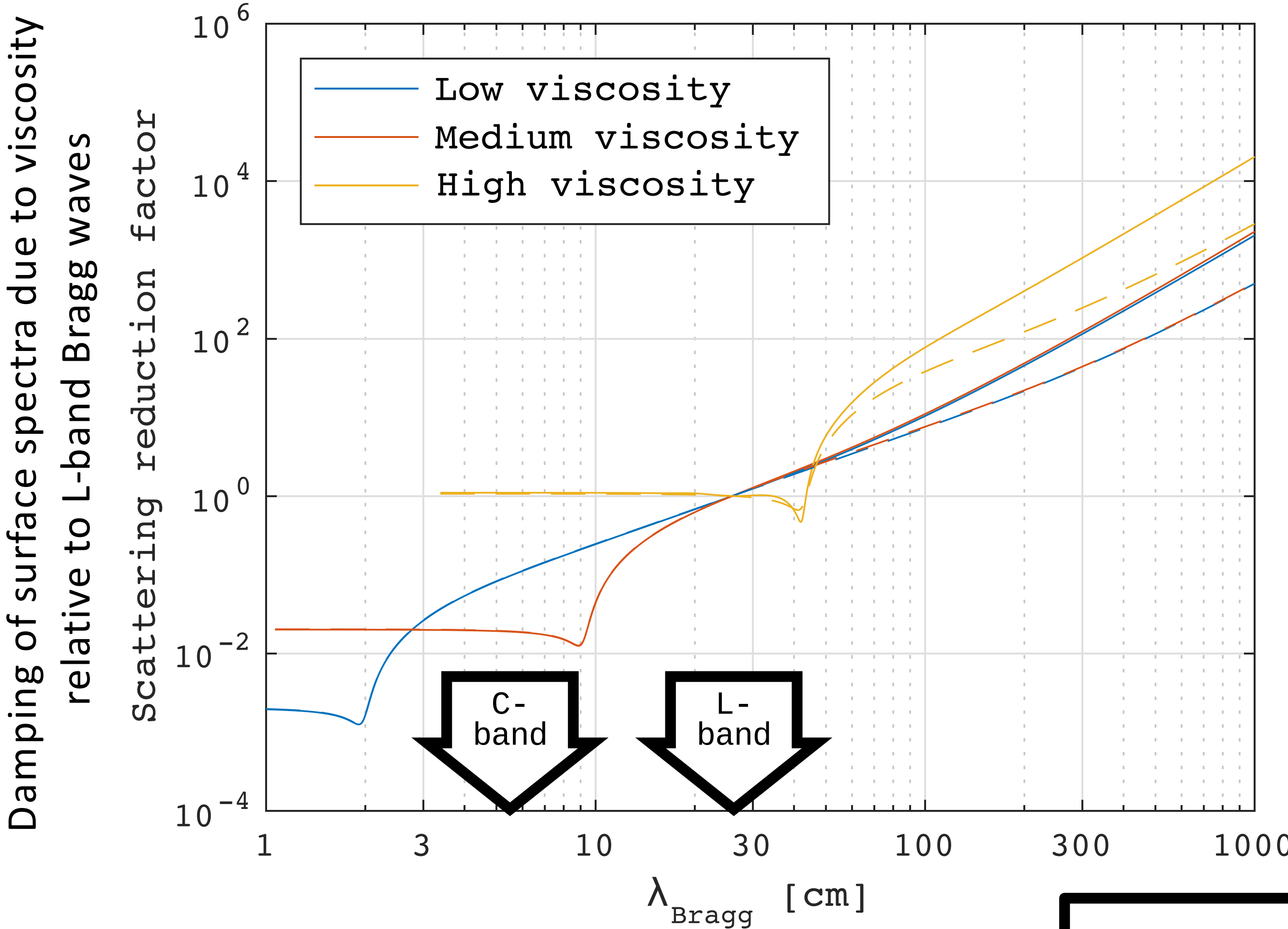

Ice modelled as viscous layer floating on top of water.

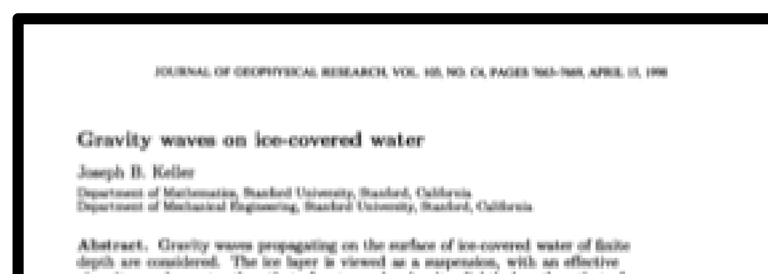
Gravity waves on ice-covered water

Joseph B. Keller

Jakob Grahn, "Sea ice remote sensing with multi-frequency radar", PhD thesis, 2018.

Topic 3: Oil spill transport – Integration of SAR and modeling


AGU PUBLICATIONS

JGR

Journal of Geophysical Research: Oceans

RESEARCH ARTICLE

Measurement and modeling of oil slick transport

Cathleen E. Jones[1], Knut-Frode Dagestad[2], Øyvind Breivik[2,3], Benjamin Holt[1], Johannes Röhrs[2], Kai Håkon Christensen[2], Martine Espeseth[4], Camilla Brekke[4], and Stine Skrunes[4]

[1]Jet Propulsion Laboratory, California Institute of Technology, Pasadena, California, USA. [2]Norwegian Meteorological Institute, Oslo, Norway. [3]University of Bergen, Geophysical Institute, Bergen, Norway. [4]Department of Physics and Technology, UiT, Arctic University of Norway, Tromsø, Norway

Key Points:
- Mineral oil and biogenic slicks are tracked using L-band SAR from release until ~8 h following during a controlled release at sea
- Simulations fit to the observations are used to refine parameters of an advanced oil transport model
- Model shows more rapid entrainment and deeper vertical transport of biogenic oil than of emulsions under high wind conditions

Abstract Transport characteristics of oil slicks are reported from a controlled release experiment conducted in the North Sea in June 2015, during which mineral oil emulsions of different volumetric ... tions and a look-alike biogenic oil were released and allowed to develop naturally. The exp... Uninhabited Aerial Vehicle Synthetic Aperture Radar (UAVSAR) to track slick location, size, a... ~8 h following release. Wind conditions during the exercise were at the high end of the ran...

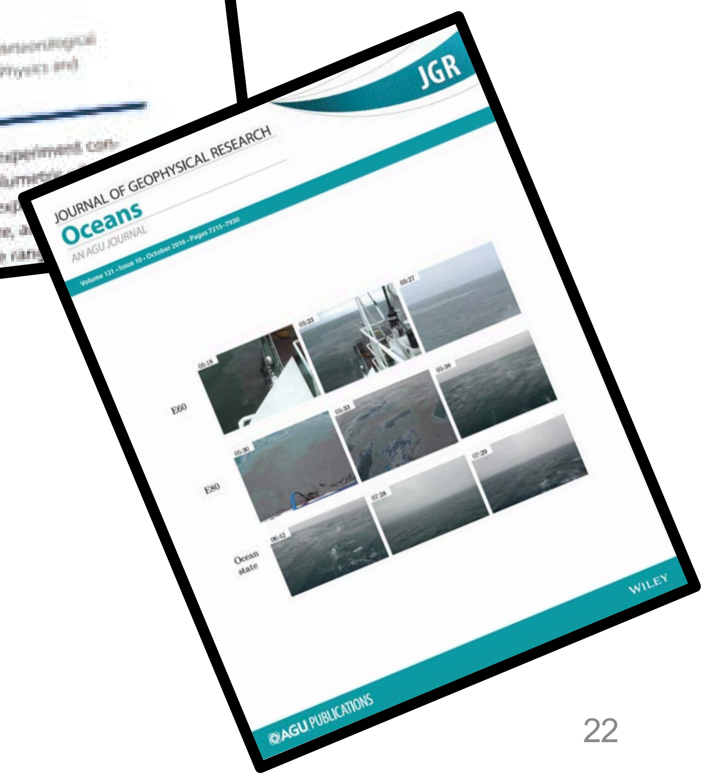

NORSE2015: NOrwegian Radar oil Spill Experiment 2015

Oil releases: 3 emulsion and 1 plant oil (biogenic slick simulator). Left untouched!
Data collection: UAVSAR, Radarsat-2, TerraSAR-X, ALOS-2, RISAT-1, photo, drifters, and weather data.

Main objectives:

- To study evolution of oil slicks
- To study transport of oil slicks
- To study oil slick detection capabilities
- To study oil slicks characterization capabilities


Radarsat-2, MDA


Stavanger, Norway


Stril Mariner: vessel conducting the releases and met/ocean observations.

Positioning of oil releases planned according to satellite imaging geometry

Release	Time (UTC)	Substance	Volume
P	04.48	Plant oil: Radiagreen ebo	0.2 m^3
E40	04.59	Emulsion (40% oil):	0.5 m^3
		300 L water + 100 L Troll + 100 L Oseberg + 0.2 L One-Mul	
E60	05.15	Emulsion (60% oil):	0.5 m^3
		200 L water + 150 L Troll + 150 L Oseberg + 0.2 L One-Mul	
E80	05.30	Emulsion (80% oil):	0.5 m^3
		100 L water + 200 L Troll + 200 L Oseberg + 0.2 L One-Mul	

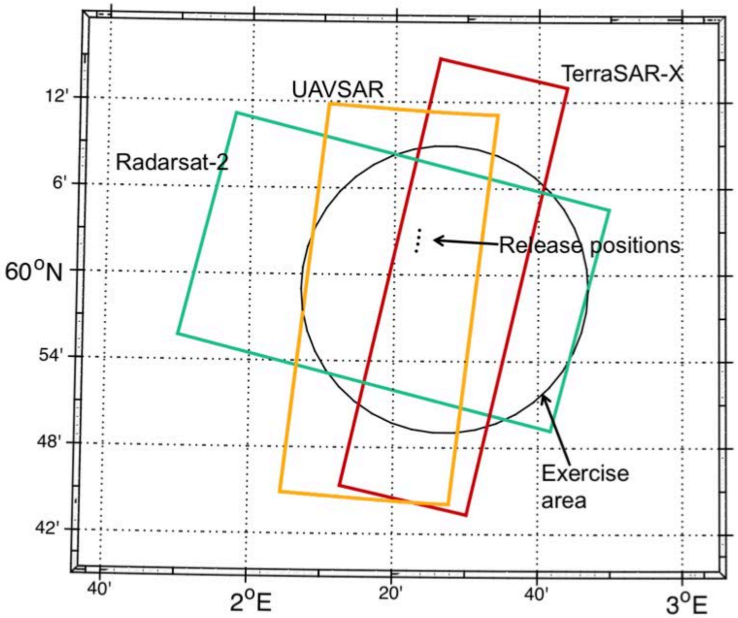

All slicks left untouched on sea surface

Timing of oil releases planned according to satellite overpass

Release	Time (UTC)	Substance	Volume
P	04.48	Plant oil: Radiagreen ebo	0.2 m^3
E40	04.59	Emulsion (40% oil): 300 L water + 100 L Troll + 100 L Oseberg + 0.2 L One-Mul	0.5 m^3
E60	05.15	Emulsion (60% oil): 200 L water + 150 L Troll + 150 L Oseberg + 0.2 L One-Mul	0.5 m^3
E80	05.30	Emulsion (80% oil): 100 L water + 200 L Troll + 200 L Oseberg + 0.2 L One-Mul	0.5 m^3

Sensor	Time (UTC)	Mode	Freq. band	Polarization
UAVSAR (16 scenes)	05.32-08.53	PolSAR	L-band	Quad-pol.
TSX	06.24	SM	X-band	Dual-pol. (HH, VV)
RS2	06.28	WFQ	C-band	Quad-pol.
RISAT-1	07.19	FRS	C-band	Compact pol. (RH, RV)
UAVSAR (6 scenes)	11.45-13.18	PolSAR	L-band	Quad-pol.
TSX	17.12	SM	X-band	Dual-pol. (HH, VV)
ALOS-2	23.53	HS	L-band	Single-pol. (VV)

The slicks were monitored by UAVSAR for 8 hours after release

- 2 flights
- 22 quad-polarimetric SAR scenes at L-band

Parameter	Value
Frequency	L-Band 1217.5 to 1297.5 MHz (23.8 cm wavelength)
Resolution	1.7 m Slant Range, 1.0 m Azimuth
Operational Altitude	12.5 km
Swatch Width	22 km
Polarization	Quad-Polarization (HH, HV, VH, VV)
Repeat Track Accuracy	± 5 meters
Transmit Power	> 3.1 kW
Radiometric Calibration	1.2 dB absolute, 0.5 dB relative
Noise Floor	-47 dB average

Comparison of multi-polarization SAR configurations in terms of signal vs. noise

TerraSAR-X (X-band)	Radarsat-2 (C-band)	UAVSAR (L-band)	RISAT-1 (C-band)
			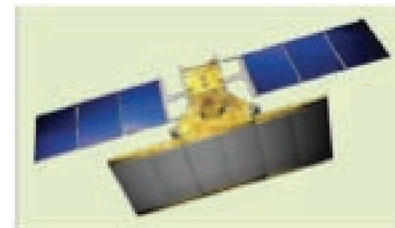

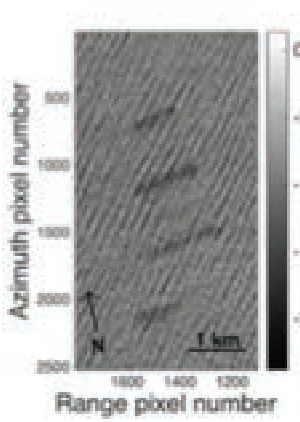

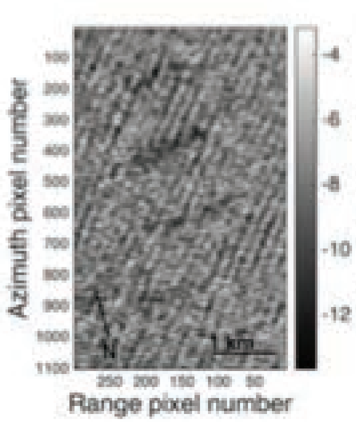

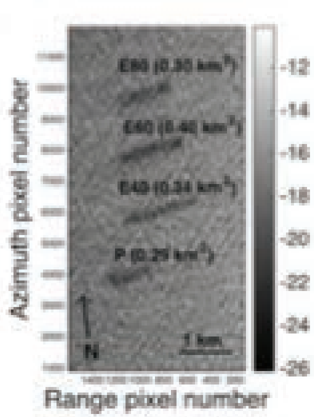

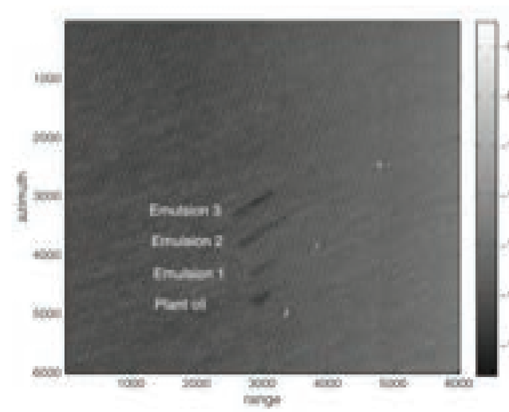

06:24 UTC	06:28 UTC	06:26-06:30 UTC	07:19 UTC

Skrunes et al., “A Multisensor Comparison of Experimental Oil Spills in Polarimetric SAR for High Wind Conditions”, IEEE JSTARS 2016.
Brekke et al., “Cross-Correlation Between Polarization Channels in SAR Imagery Over Oceanographic Features”, IEEE GRSL 2016.

Noise floor

TerraSAR-X Radarsat-2 UAVSAR

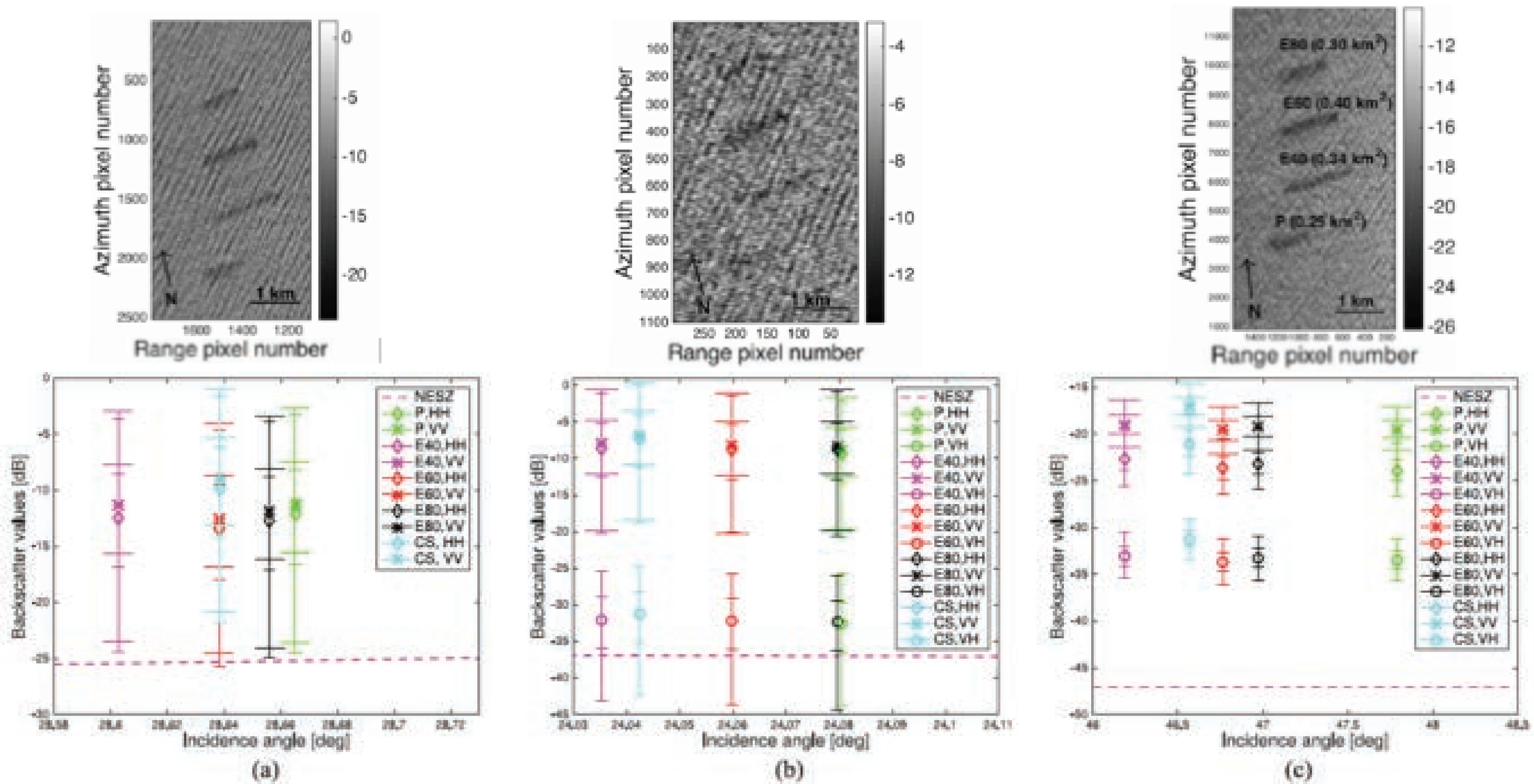

Fig. 5. Noise analyses. (a) TSX. (b) RS2. (c) UAVSAR. For each ROI, the horizontal lines indicate the 5th, 25th, 75th, and 95th percentiles, and the 50th percentile is indicated by a symbol, depending on the polarization channel. The VV lines are a little wider than those for HH and VH. CS indicates clean sea.

Skrunes et al., "A Multisensor Comparison of Experimental Oil Spills in Polarimetric SAR for High Wind Conditions", IEEE JSTARS 2016.

Drifters were released at P and E80 to provide position and sea surface temperature at 10 min intervals

Photo: Øyvind Breivik

<u>Drifters:</u>

- 2 iSphere (subject to direct wind drift)
- 2 Self Locating Datum Marker Buoy (submerged)

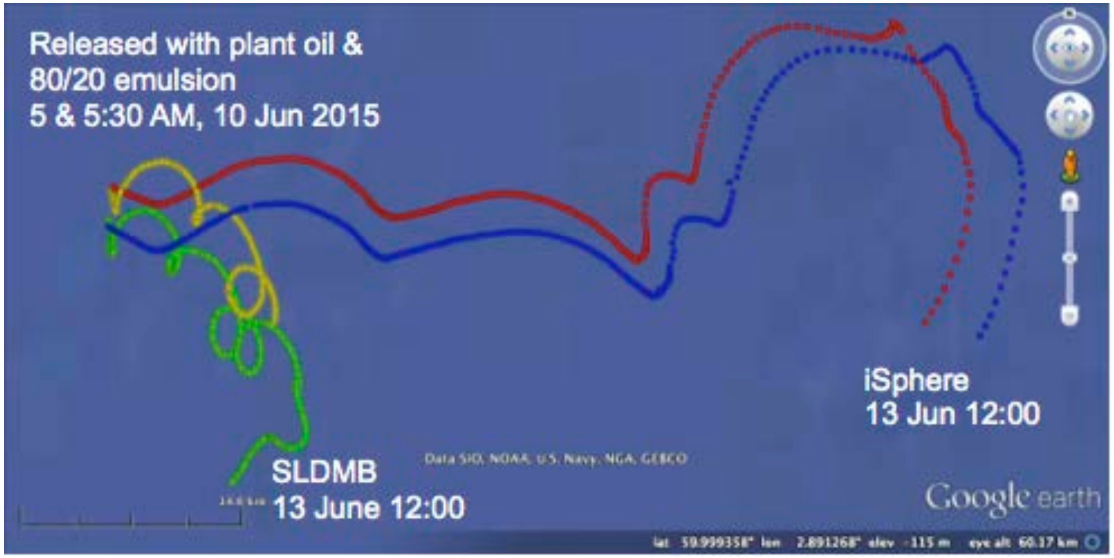

Releases were left to develop under relatively high sea state with winds in the range 9–12 m/s

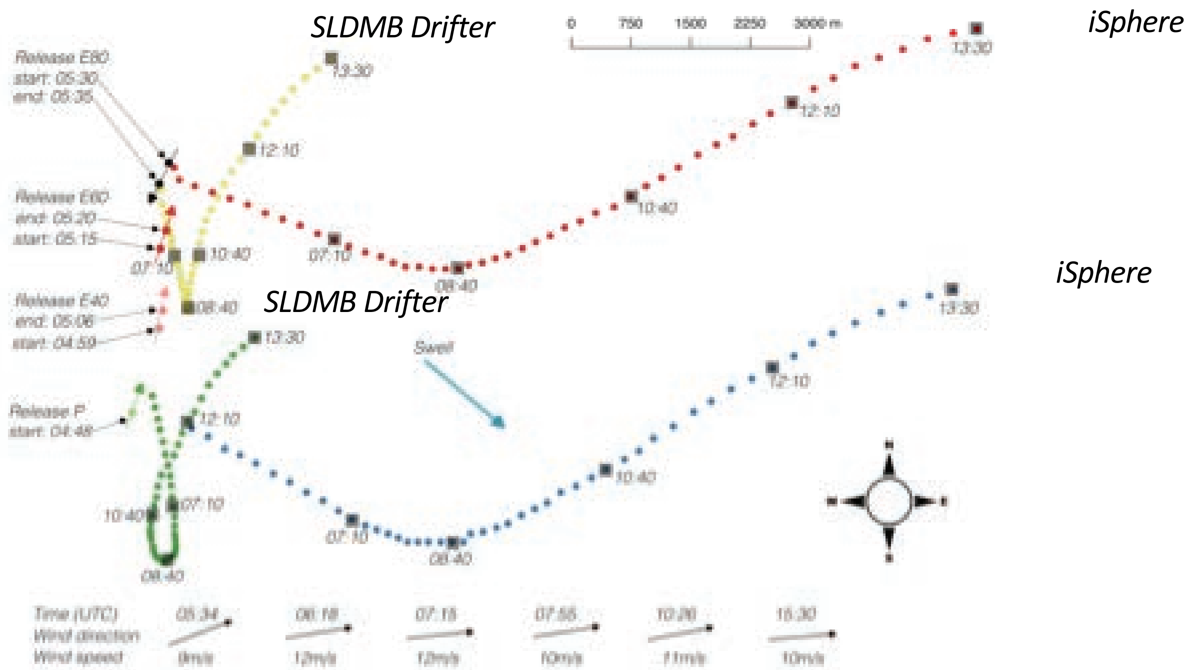

Ocean state

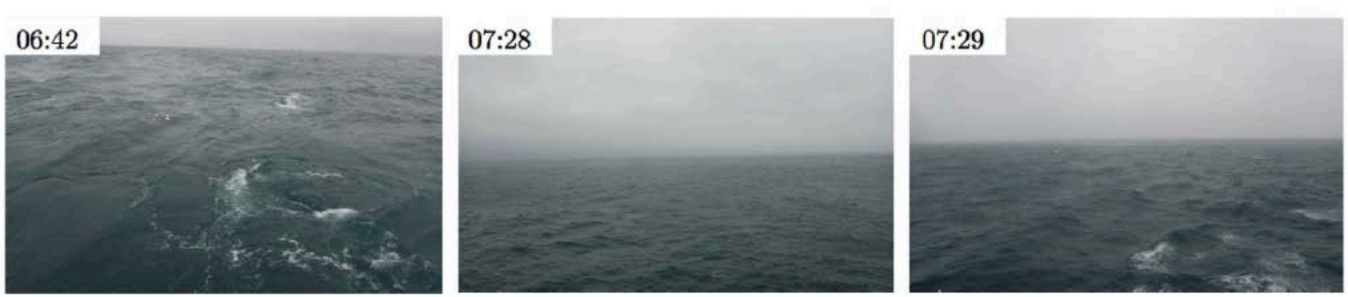

Time series of UAVSAR used to get position and size of evolving slicks

From UAVSAR: Relative position, extent, and spread in the 8 h following release

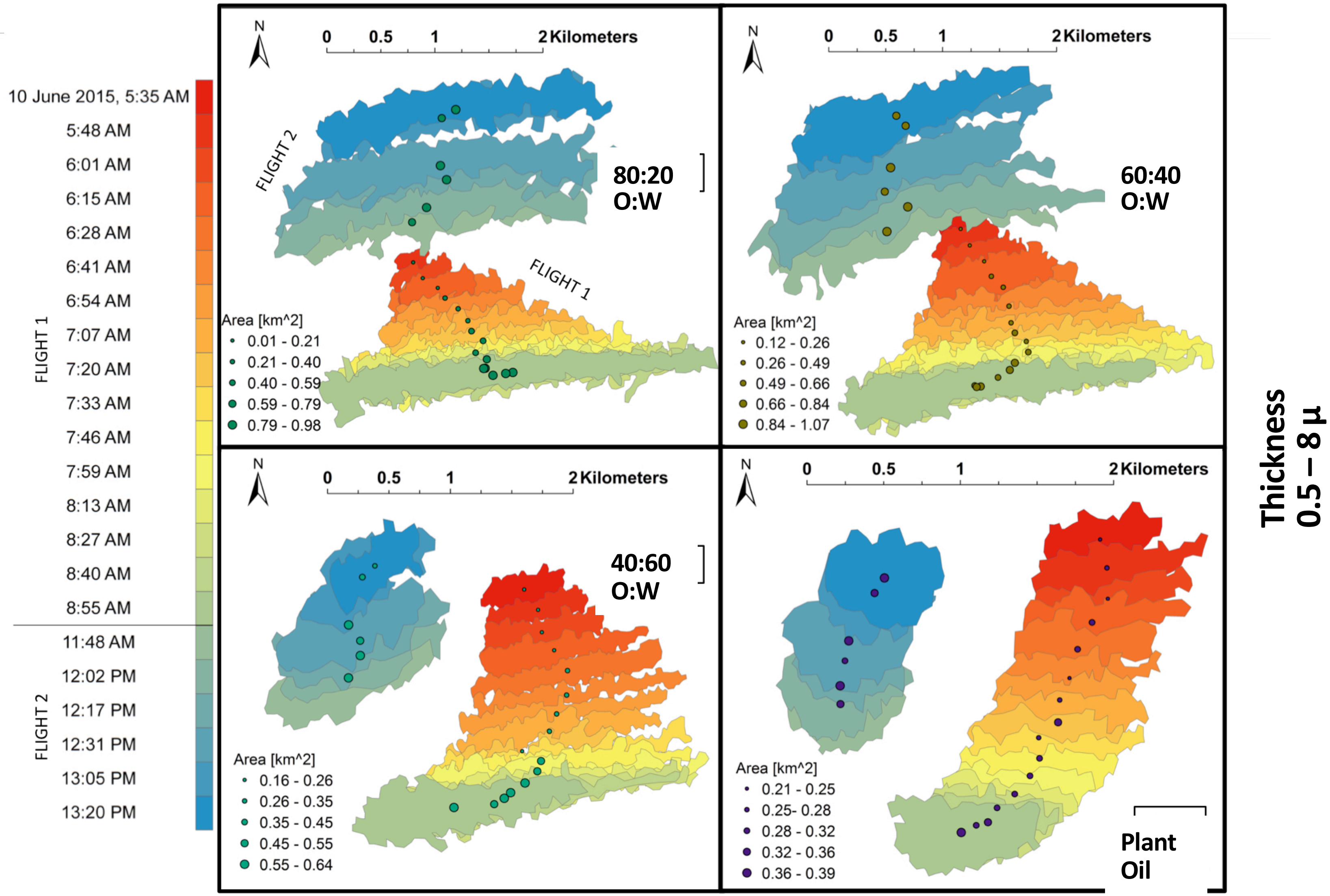

Parameters in Met Norway’s OpenOil drift model tuned to fit UAVSAR measurements

→ Oil represented by particles (seeded within contours from UAVSAR)

→ Simulated transport of P and E80 (slicks with associated iSphere and SLDMB drifters).

Horizontal movement:

- Ambient current (two runs: SLDMB drifters or model)
- Wave-induced Stokes drift
- Windage (~2% of surface wind)

Vertical movement:

- Entrainment of oil surface elements by breaking waves
- Eddy diffusivity of submerged droplets (random walk scheme)
- Rise of submerged particles due to buoyancy

Two free parameters:

- Entrainment rate
- Droplet radius

Trajectories show particles spending most time close to (far below) surface drift faster eastward (westward)

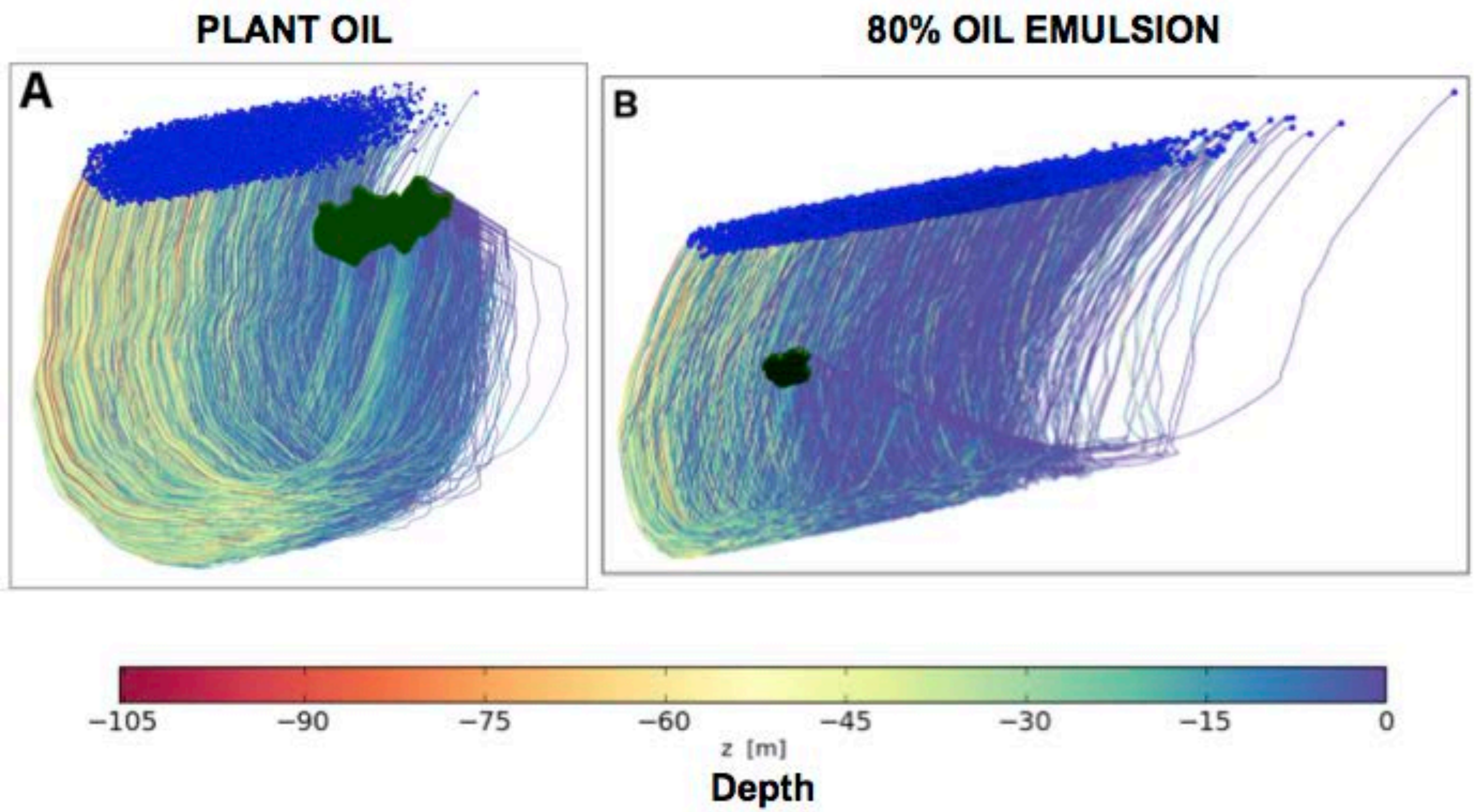

Bulk of plant oil below surface shielded from strong eastward Stokes drift and surface wind.
Trajectory mainly steered by currents and in agreement with UAVSAR observations.

Difference in depth profiles found, indicating a potential for slick discrimination based on transport

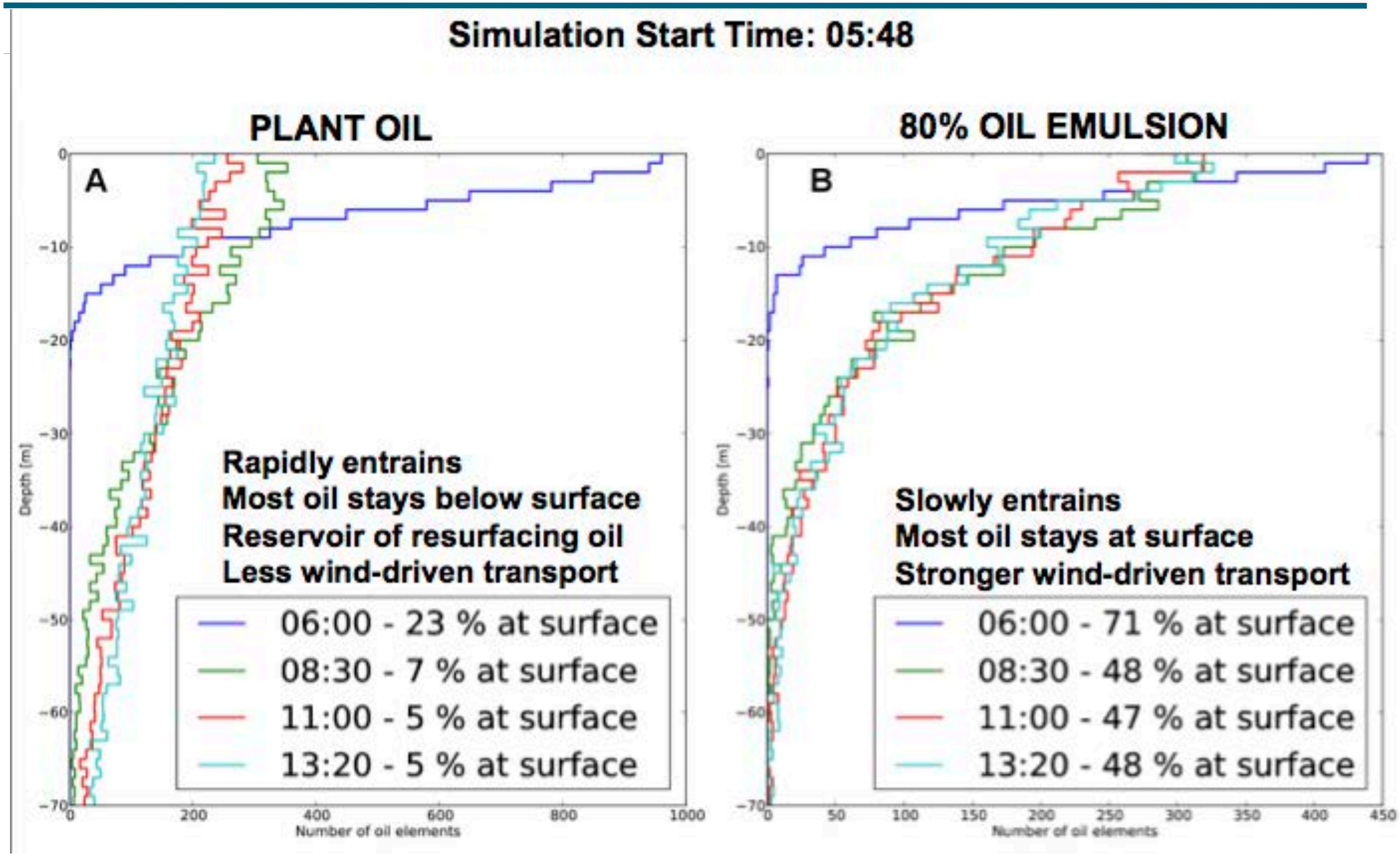

Key message to take home

Plant oil:

→ Rapidly entrains

→ Most oil stays below surface

→ Reservoir of resurfacing oil

→ Less wind-driven transport

Mineral oil emulsion (80%)

→ Slowly entrains

→ Most oil stays at surface

→ Stronger wind-driven transport

Careful planning and interdisciplinary research team key factors for success!